

# Rare earth element doping effect on the bonding and the transport property of $\delta$ -MoN

Jing Yu · Guiling Zhang · Yan Shang ·  
Hui Zhang · Luqing Yang · Tao Zeng ·  
Bo Liu · Zesheng Li

Received: 5 July 2010/Accepted: 25 October 2010/Published online: 21 November 2010  
© Springer-Verlag 2010

**Abstract** Combining non-equilibrium Green's function technique with density functional theory, the rare earth element doping effect on the bonding and the transport property of  $\delta$ -MoN were theoretically investigated. The Mo–N bond lengths become more uneven after dopings. Some Mo–N bonds were heavily lengthened by the La- and Gd-dopings, resulting in obvious damages of their bonding. Evident covalent-like La–N and Gd–N bonds were formed in La–MoN and Gd–MoN, respectively, while the Yb atom underwent an ionic-like interaction with its neighboring N atoms in Yb–MoN. A clear drop of the conductivity was found after La- and Gd-dopings. On the contrary, the conductivity was improved upon the Yb-doping. This case was rationalized from the carrier density and the scattering of the carriers. The backscattering effect was evident at the impurities. The La- and Gd-dopings could not effectively increase the carrier density near the Fermi level, while the Yb atom could offer *f*-carriers to transfer from the valence band to the conduction band.

**Electronic supplementary material** The online version of this article (doi:[10.1007/s00214-010-0845-0](https://doi.org/10.1007/s00214-010-0845-0)) contains supplementary material, which is available to authorized users.

J. Yu · G. Zhang (✉) · Y. Shang · H. Zhang · L. Yang ·  
T. Zeng (✉) · B. Liu

College of Chemical and Environmental Engineering,  
Harbin University of Science and Technology,  
150080 Harbin, People's Republic of China  
e-mail: zglhrb@163.com

T. Zeng  
e-mail: taozeng2008@163.com

Z. Li  
Institute of Theoretical Chemistry, State Key Laboratory  
of Theoretical and Computational Chemistry, Jilin University,  
130023 Changchun, People's Republic of China

**Keywords** Rare earth element · Doping effect ·  $\delta$ -MoN · Theoretical study

## 1 Introduction

Molybdenum nitride, a typical transition metal nitride, is known to have a set of interesting physical properties such as low compressibility, high melting point, magnetism, and superconductivity [1–7]. In experiments, three stable phases have been found for molybdenum nitride:  $\delta$ -MoN (hexagonal),  $\gamma$ -Mo<sub>2</sub>N (cubic), and  $\beta$ -Mo<sub>2</sub>N (tetragonal) [8–12]. Metathesis reactions such as MoO<sub>3</sub> + NH<sub>4</sub>Cl or Zn<sub>3</sub>N<sub>2</sub> + MoCl<sub>3</sub> can yield either  $\delta$ -MoN or  $\gamma$ -Mo<sub>2</sub>N, depending upon the synthesis conditions and the choice of precursors [13].  $\gamma$ -Mo<sub>2</sub>N can convert into  $\delta$ -MoN when it is heated under the condition of high N<sub>2</sub> activity. Many studies have reported the synthesis and characteristics of  $\gamma$ -Mo<sub>2</sub>N [14–16]. The literatures concerning the synthesis of  $\beta$ -Mo<sub>2</sub>N are relatively scarce probably owing to its easy transformation to  $\gamma$ -Mo<sub>2</sub>N [11, 17]. In addition, a metastable phase with cubic NaCl type structure (so called *B1*-MoN) has also been experimentally explored [18–23].

A few theoretical works have been devoted to molybdenum nitride, while most of them have focused on the stoichiometric NaCl phase of *B1*-MoN. In the early 1980 s, theoretical calculations predicted that *B1*-MoN would possess a high superconducting transition temperature of about 29 K [24–27]. Using the linear-augmented plane-wave method, Gus et al. found in 2000 that the elastic instability in *B1*-structure MoN persisted at elevated pressures, offering little hope of stabilizing this material without chemical doping [28]. In recent years, the density functional theory (DFT) has been used to calculate  $\delta$ -MoN. Some important conclusions concerning the cohesive

energy, electronic bands, bulk modulus, structural stability, and mechanical properties have been achieved [29, 30]. Molybdenum nitride is a typical metallic material. However, to the best of our knowledge, no theoretical literatures have been related to the transport property.

A general strategy for tuning the property of materials is by the doping with alien atoms. The rare earth elements, Ln, are known to have a set of interesting properties due to their special  $f$ -electronic structures. In this paper, we selected  $\delta$ -MoN as studied target to investigate the rare earth element doping effect on the bonding and the transport property. In  $\delta$ -MoN, Mo atoms have two kinds of lattice points: one is labeled 6c and the other is labeled 2a in the International Tables. Three special rare earth elements, La with empty  $f^0$  structure, Gd with half-filled  $f^7$  structure, and Yb with full-filled  $f^{14}$  structure, were used as dopants to substitute the 6c Mo (denoted as Ln–MoN(6c)) and the 2a Mo (denoted as Ln–MoN(2a)), respectively. We have found that the electronic structure and the transport property of Ln–MoN(2a) are rather similar to those of corresponding Ln–MoN(6c), so in the following sections, we mainly focus on the Ln-doping effect at the 6c position. The results of Ln–MoN(2a) are given in the Supporting Information (Table S1 and Figure S1–S6). This work may offer some clues for understanding the impurity effect on the transport property of other transition metal nitride.

Although  $\delta$ -MoN with its hexagonal structure has been experimentally known for some time [12], the quality of the crystal was not sufficiently good to determine the exact positions of the lattice atoms. The space groups of P-3 ml(164), P6<sub>3</sub>/mmc(194), and P6<sub>3</sub>mc(186) have been all mentioned for  $\delta$ -MoN in the literatures [9, 12, 31]. Molecular dynamic simulations have suggested that the stable structure of  $\delta$ -MoN preferred to be P6<sub>3</sub>mc(186) symmetry [32]. Recently, the positions of the perfectly ordered Mo and N atoms with P6<sub>3</sub>mc(186) symmetry have been revealed by the X-ray and the neutron diffraction experiments [11, 33]. In this paper, the P6<sub>3</sub>mc(186) symmetry of  $\delta$ -MoN was employed to study the rare earth element doping effect on the bonding and the transport property.

## 2 Computational details

### 2.1 VASP calculations

The unit cell of the undoped  $\delta$ -MoN is shown in Fig. 1, in which the Mo atoms and the N atoms are labeled, respectively. Each repeated unit contains 8 formula units of MoN. In this paper, the center Mo<sub>1</sub> atom (6c position) and the side Mo<sub>7</sub> atom (2a position) were substituted, respectively, by the rare earth element to carry out VASP

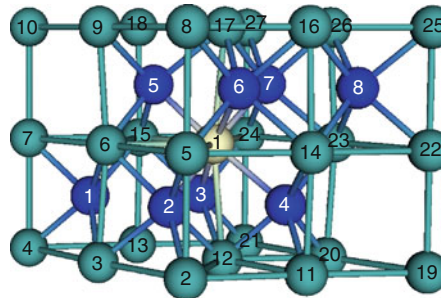


**Fig. 1** The unit cell of  $\delta$ -MoN. The green and blue balls denote the Mo and the N atoms, respectively. The yellow ball denotes the Mo atom in  $\delta$ -MoN and denotes the Ln atom in Ln–MoN(6c)

calculations for investigating the Ln-doping effects on the geometric and electronic structures.

The calculations were performed in the SGI 3800 workstation with the program package of VASP [34], which was developed at the Institut für Theoretische Physik of Technische Universität Wien. Structural optimizations were carried out in the framework of DFT within the generalized gradient approximation (GGA) [35]. The Perdew and Wang parametrization (PW91) [36] was adopted for the exchange-correlation potential. The electron-ion interaction was represented by projector-augmented wave (PAW) potentials [37, 38]. Two cutoff energies, 350 and 400 eV, were used to relax the geometry of La–MoN(6c). The calculated results are listed in Table 1. It is found that the bond lengths obtained from 350 eV cutoff energy are in good agreement with those from 400 eV cutoff energy with the maximum deviation of only 0.02 Å. Therefore, 350 eV cutoff energy was applied to describe the electron wave function for the easier convergence of other Ln–MoN. Sampling of the irreducible wedge of the Brillouin zone was performed with regular  $5 \times 5 \times 5$  Monkhorst–Pack grid of special points. The spin-polarized calculations were carried out for both of the undoped and doped species. The atomic positions, the lattice constants, and the unit cell volumes were all optimized so as to get a minimum of the total energy. The optimized structures of the undoped  $\delta$ -MoN are listed in Table 2, where we can see that the calculated lattice parameters, the nearest neighbor distances, and the atomic positions show small deviation from the experimental observations, indicating that our simulation methodology was reasonable.

Using the relaxed structures, we calculated the electronic structures of the undoped  $\delta$ -MoN and the doped Ln–MoN, including the band structures, the total densities of states (TDOS), and the projected densities of states (PDOS). To account better for the on-site  $f$ -electron correlations of the rare earth elements, we further employed

**Table 1** Comparison of bond lengths between 350 and 400 eV cutoff energies obtained from VASP relaxations on La–MoN(6c)

Bonds	Bond lengths (Å)	
	350 eV	400 eV
La <sub>1</sub> –N <sub>2</sub>	2.46	2.45
La <sub>1</sub> –N <sub>3</sub>	2.46	2.45
La <sub>1</sub> –N <sub>4</sub>	2.42	2.41
La <sub>1</sub> –N <sub>5</sub>	2.42	2.41
La <sub>1</sub> –N <sub>6</sub>	2.41	2.40
La <sub>1</sub> –N <sub>7</sub>	2.41	2.40
Mo <sub>3</sub> –N <sub>1</sub>	2.29	2.31
Mo <sub>4</sub> –N <sub>1</sub>	2.00	2.00
Mo <sub>6</sub> –N <sub>1</sub>	2.14	2.14
Mo <sub>13</sub> –N <sub>1</sub>	2.29	2.31
Mo <sub>15</sub> –N <sub>1</sub>	2.14	2.14
Mo <sub>2</sub> –N <sub>2</sub>	2.10	2.10
Mo <sub>3</sub> –N <sub>2</sub>	2.27	2.25
Mo <sub>5</sub> –N <sub>2</sub>	2.37	2.38
Mo <sub>6</sub> –N <sub>2</sub>	2.09	2.08
Mo <sub>12</sub> –N <sub>2</sub>	2.20	2.20
Mo <sub>12</sub> –N <sub>3</sub>	2.20	2.20
Mo <sub>13</sub> –N <sub>3</sub>	2.27	2.25
Mo <sub>15</sub> –N <sub>3</sub>	2.09	2.08
Mo <sub>21</sub> –N <sub>3</sub>	2.10	2.10
Mo <sub>24</sub> –N <sub>3</sub>	2.37	2.38
Mo <sub>11</sub> –N <sub>4</sub>	2.03	2.04
Mo <sub>12</sub> –N <sub>4</sub>	2.13	2.13
Mo <sub>14</sub> –N <sub>4</sub>	2.45	2.44
Mo <sub>20</sub> –N <sub>4</sub>	2.03	2.04
Mo <sub>23</sub> –N <sub>4</sub>	2.45	2.44
Mo <sub>15</sub> –N <sub>5</sub>	2.10	2.11
Mo <sub>6</sub> –N <sub>5</sub>	2.10	2.11
Mo <sub>9</sub> –N <sub>5</sub>	2.21	2.21
Mo <sub>17</sub> –N <sub>5</sub>	2.41	2.40
Mo <sub>18</sub> –N <sub>5</sub>	2.21	2.21
Mo <sub>5</sub> –N <sub>6</sub>	2.22	2.22
Mo <sub>8</sub> –N <sub>6</sub>	2.09	2.10
Mo <sub>14</sub> –N <sub>6</sub>	2.37	2.38
Mo <sub>16</sub> –N <sub>6</sub>	2.03	2.03
Mo <sub>17</sub> –N <sub>6</sub>	2.19	2.19
Mo <sub>17</sub> –N <sub>7</sub>	2.19	2.19
Mo <sub>23</sub> –N <sub>7</sub>	2.37	2.38
Mo <sub>24</sub> –N <sub>7</sub>	2.22	2.22
Mo <sub>26</sub> –N <sub>7</sub>	2.03	2.03
Mo <sub>27</sub> –N <sub>7</sub>	2.09	2.10
Mo <sub>14</sub> –N <sub>8</sub>	2.23	2.24
Mo <sub>16</sub> –N <sub>8</sub>	2.12	2.13
Mo <sub>22</sub> –N <sub>8</sub>	2.04	2.03
Mo <sub>23</sub> –N <sub>8</sub>	2.23	2.24
Mo <sub>26</sub> –N <sub>8</sub>	2.12	2.13

**Table 2** Comparison of lattice parameters, nearest neighbor distances, and atomic positions of δ-MoN between experiment investigations and calculated results

δ-MoN	Lattice parameter (Å)			Nearest neighbor distance (Å)	
	a	c	c/a	Mo <sub>1</sub> –N <sub>4,5</sub>	Mo <sub>1</sub> –N <sub>2,3,6,7</sub>
Calculation	5.777	5.673	0.982	2.19 (2.20)	2.17 (2.22)
Experiment <sup>a</sup>	5.731	5.609	0.979	2.05 (2.17)	2.04 (2.17)

Atoms	Calculation	Experiment <sup>a</sup>
Atomic positions		
Mo <sub>1</sub>	(0.4879, 0.5120, 0.4984)	(0.5082, 0.4918, 0.4936)
Mo <sub>7</sub>	(0, 0, 0.5048)	(0, 0, 0.5)
N <sub>4,5</sub>	(0.3333, 0.6667, 0.7715)	(0.3333, 0.6667, 0.7993)
N <sub>1–3,6–8</sub>	(0.1669, 0.8330, 0.2428)	(0.1643, 0.8357, 0.2813)

N<sub>4,5</sub> and N<sub>1–3,6–8</sub> locate at 2b and 6c positions in the International Tables, respectively. Two Mo<sub>1</sub>–N(2b/6c) bond lengths are found from theoretical and experimental results

<sup>a</sup> Reference [11]

the GGA + U approach [39] to calculate the electronic structures of the relaxed Ln–MoN. At the GGA + U level, the total energy can be described by the following expression [40]:

$$E^{\text{GGA+U}} = E^{\text{GGA}} + \frac{\overline{U} - \overline{J}}{2} \sum_{\sigma} \left[ \left( \sum_m n_{m,m}^{\sigma} \right) - \left( \sum_{m,m'} n_{m,m'}^{\sigma} n_{m',m}^{\sigma} \right) \right] \quad (1)$$

where  $\overline{U}$  and  $\overline{J}$  are the spherically averaged matrix elements of the screened Coulomb electron–electron interaction, and  $n$  is the density matrix of  $f$ -electrons.  $m$  and  $m'$  denote different  $f$ -orbitals, and  $\sigma$  is the spin index. It is convenient to define an effective interaction parameter as  $U_{\text{eff}} = \overline{U} - \overline{J}$ , since the total energies are insensitive to  $\overline{J}$  when  $U_{\text{eff}}$  is fixed. In the calculations, we used  $U_{\text{eff}} = 6$  eV for Ln  $f$ -orbitals.

## 2.2 ATK calculations

The electronic transport property was calculated using an ab initio code package, Atomistix ToolKit (ATK), which is based on the combination of the Keldysh non-equilibrium Green's function (NEGF) formalism and the DFT [41–44]. Based on the VASP-relaxed structures, two-probe systems were constructed. Figure 2 schematically shows the model of the two-probe system, which could be divided into three parts: the left electrode, the scattering region, and the right electrode. The scattering region consists of four unit cells of δ-MoN or Ln–MoN and two layers of surface atoms at each side of the electrode interface. The structure of the two-probe system is Ag(111)/δ-MoN(001)/Ag(111) or

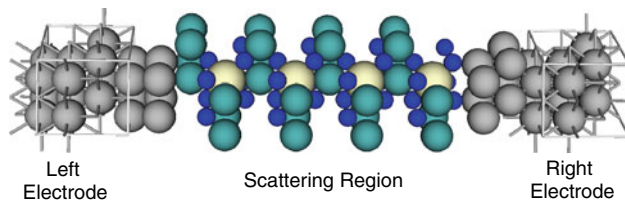


**Fig. 2** The two-probe systems of the undoped  $\delta$ -MoN and the doped Ln–MoN(6c) self-assembled on the Ag (111) surface. The chains together with two surface silver layers in the left and right electrodes are included in the self-consistent calculation, while the remainders of the silver electrodes are atoms described by employing bulk Hamiltonian parameters and self-energies on Ag in the electrode region. The positive applied bias corresponds to that the current flows from the *left* to the *right* electrode and the negative applied bias corresponds to that the current flows from the *right* to the *left* electrode. The green and blue balls denote the Mo and the N atoms, respectively. The yellow ball denotes the Mo atom in  $\delta$ -MoN and denotes the Ln atom in Ln–MoN(6c)

Ag(111)/Ln–MoN(001)/Ag(111). For the sake of a relative comparison between these studied models, the same electrode structures are needed for all the two-probe systems. The lattice constants,  $a$  and  $b$ , of the Ag electrode are 5.778 Å in the database of the ATK program. In order to make a good match between the electrode and the scattering intermedia, the lattice constants of the undoped  $\delta$ -MoN and the doped Ln–MoN were also set to be the same as the electrode. To obtain quantum-mechanically stable structures, the atomic positions in the scattering regions were relaxed within a force convergence criterion of 0.06 eV/Å.

Calculations were carried out by changing the applied bias by the step of 0.2 V in the range of –1.0 to 1.0 V. The local density approximation (LDA) in the form of Perdew–Zunger exchange-correlation functional was used. Core electrons were described by norm-conserving pseudopotentials, and valance electrons were expanded in a basis set of single-zeta plus polarization (SZP). The total energy was well converged within 1–2 meV/atom with a cutoff energy of 100 Ry and a  $3 \times 3 \times 50$  k-point sampling.

### 3 Results and discussions

In this section, we first focus on the Ln-doping effect on the geometry and the bonding, and then, we take into account the Ln-doping effect on the transport property. Here, we mainly concentrate on Ln–MoN(6c) owing to the similarities between Ln–MoN(6c) and Ln–MoN(2a) in the electronic structure and the transport property. The results of Ln–MoN(2a) are given as Supporting Information (Table S1 and Figure S1–S6). Following, we appoint Ln–MoN(6c) to be Ln–MoN for simplicity.

#### 3.1 Effect on the geometry and the bonding

Dopants would inevitably alter the geometry that is an important factor for varying the bonding. The optimized bond lengths of Mo–N and Ln–N bonds are given in Table 3. The  $\text{Ln}_1\text{--N}$  bond lengths are longer than the  $\text{Mo}_1\text{--N}$  bond lengths, which is due to the fact that the radii of  $\text{Ln}^{3+}$  ( $\text{La}^{3+}$ : 1.22,  $\text{Gd}^{3+}$ : 1.11, and  $\text{Yb}^{3+}$ : 1.00 Å) are larger than  $\text{Mo}^{3+}$  (0.68 Å). The average bond length of  $\text{Mo}_1\text{--N}$  is 2.20 Å while those of  $\text{La}_1\text{--N}$ ,  $\text{Gd}_1\text{--N}$ , and  $\text{Yb}_1\text{--N}$  go up to 2.43, 2.32, and 2.30 Å, respectively. Such lengthening of the Ln–N bond consequentially leads to the expansion of the unit cell which can be reflected from the unit cell parameters and the unit cell volumes as given in Table 4.

The presence of the rare earth atom has a marked effect upon the Mo–N bonds. In the parent  $\delta$ -MoN, the Mo–N bond lengths are not identical due to the different coordination orientation between the Mo  $d$ -orbitals and the N  $p$ -orbitals. The Mo–N bond lengths are 2.15–2.24 for  $\delta$ -MoN, 2.00–2.45 for La–MoN, 2.02–2.36 for Gd–MoN, and 2.02–2.40 Å for Yb–MoN. Apparently, the Mo–N bond lengths become more uneven after Ln-doping. Incorporating of an impurity could induce some Mo–N bond lengths increase and some decrease. A similar changing trend is found for a given Mo–N bond regardless of what kind of doping. For example, all the  $\text{Mo}_3\text{--N}_1$  bonds are elongated and all the  $\text{Mo}_4\text{--N}_1$  bonds are shortened under three kinds of Ln-dopings. It is worth noticed that the longest Mo–N bond, 2.24 Å, occurs at the  $\text{N}_{2,3,6,7}$  atoms in the undoped  $\delta$ -MoN, while it occurs at the  $\text{N}_{4,5}$  atoms in the doped Ln–MoN. Upon doping, the  $\text{Mo}_{14,23}\text{--N}_4$  bonds become to be the longest: 2.45 for La–MoN, 2.36 for Gd–MoN, and 2.40 Å for Yb–MoN and followed is the  $\text{Mo}_{17}\text{--N}_5$  bond: 2.41 for La–MoN, 2.35 for Gd–MoN, and 2.32 Å for Yb–MoN (c.f. Table 3). Such elongation predictively weakens their bond strengths, which will be further confirmed by the charge-density distribution. In addition, the changed magnitude of the Mo–N bond length does not follow the sequence of the La-, Gd-, and Yb-doping. For example, the  $\text{Mo}_{24}\text{--N}_3$  bond is lengthened by 0.13 and 0.09 Å after the La-doping and the Yb-doping, respectively, while it is only elongated by 0.01 Å after the Gd-doping.

The distinct distortion of the geometry raised by the Ln-doping stimulates our interest to investigate the stability of the Ln–MoN systems. We calculated the formation energy of Ln–MoN,  $E_f^{\text{Ln}}$ , by the following formula [45]:

$$E_f^{\text{Ln}} = E_{\text{tot}}^{\text{Ln--MoN}} - E_{\text{tot}}^{\text{MoN}} + \mu_{\text{Mo}} - \mu_{\text{Ln}} \quad (2)$$

where  $E_{\text{tot}}^{\text{Ln--MoN}}$  and  $E_{\text{tot}}^{\text{MoN}}$  are the total energies of the Ln–MoN and  $\delta$ -MoN, respectively.  $\mu_{\text{Mo}}$  ( $\mu_{\text{Ln}}$ ) is the chemical potential of the Mo (Ln) atom.

**Table 3** The VASP-optimized bond lengths ( $\text{\AA}$ ) for  $\delta$ -MoN and Ln–MoN(6c)

Bonds	$\delta$ -MoN	La–MoN(6c)	Gd–MoN(6c)	Yb–MoN(6c)
Mo <sub>1</sub> –N <sub>2</sub>	2.17			
Mo <sub>1</sub> –N <sub>3</sub>	2.17			
Mo <sub>1</sub> –N <sub>4</sub>	2.20			
Mo <sub>1</sub> –N <sub>5</sub>	2.19			
Mo <sub>1</sub> –N <sub>6</sub>	2.22			
Mo <sub>1</sub> –N <sub>7</sub>	2.22			
La <sub>1</sub> –N <sub>2</sub>		2.46		
La <sub>1</sub> –N <sub>3</sub>		2.46		
La <sub>1</sub> –N <sub>4</sub>		2.42		
La <sub>1</sub> –N <sub>5</sub>		2.42		
La <sub>1</sub> –N <sub>6</sub>		2.41		
La <sub>1</sub> –N <sub>7</sub>		2.41		
Gd <sub>1</sub> –N <sub>2</sub>			2.33	
Gd <sub>1</sub> –N <sub>3</sub>			2.33	
Gd <sub>1</sub> –N <sub>4</sub>			2.33	
Gd <sub>1</sub> –N <sub>5</sub>			2.31	
Gd <sub>1</sub> –N <sub>6</sub>			2.32	
Gd <sub>1</sub> –N <sub>7</sub>			2.32	
Yb <sub>1</sub> –N <sub>2</sub>				2.37
Yb <sub>1</sub> –N <sub>3</sub>				2.37
Yb <sub>1</sub> –N <sub>4</sub>				2.26
Yb <sub>1</sub> –N <sub>5</sub>				2.31
Yb <sub>1</sub> –N <sub>6</sub>				2.25
Yb <sub>1</sub> –N <sub>7</sub>				2.25
Mo <sub>3</sub> –N <sub>1</sub>	2.22	2.29	2.27	2.25
Mo <sub>4</sub> –N <sub>1</sub>	2.15	2.00	2.02	2.02
Mo <sub>6</sub> –N <sub>1</sub>	2.17	2.14	2.13	2.14
Mo <sub>13</sub> –N <sub>1</sub>	2.22	2.29	2.27	2.25
Mo <sub>15</sub> –N <sub>1</sub>	2.17	2.14	2.13	2.14
Mo <sub>2</sub> –N <sub>2</sub>	2.15	2.10	2.17	2.15
Mo <sub>3</sub> –N <sub>2</sub>	2.22	2.27	2.27	2.19
Mo <sub>5</sub> –N <sub>2</sub>	2.24	2.37	2.25	2.30
Mo <sub>6</sub> –N <sub>2</sub>	2.17	2.09	2.10	2.07
Mo <sub>12</sub> –N <sub>2</sub>	2.22	2.20	2.23	2.16
Mo <sub>12</sub> –N <sub>3</sub>	2.22	2.20	2.23	2.16
Mo <sub>13</sub> –N <sub>3</sub>	2.22	2.27	2.27	2.19
Mo <sub>15</sub> –N <sub>3</sub>	2.17	2.09	2.10	2.07
Mo <sub>21</sub> –N <sub>3</sub>	2.15	2.10	2.17	2.15
Mo <sub>24</sub> –N <sub>3</sub>	2.24	2.37	2.25	2.33
Mo <sub>11</sub> –N <sub>4</sub>	2.19	2.03	2.08	2.04
Mo <sub>12</sub> –N <sub>4</sub>	2.19	2.13	2.12	2.07
Mo <sub>14</sub> –N <sub>4</sub>	2.20	2.45	2.36	2.40
Mo <sub>20</sub> –N <sub>4</sub>	2.19	2.03	2.08	2.04
Mo <sub>23</sub> –N <sub>4</sub>	2.20	2.45	2.36	2.40
Mo <sub>15</sub> –N <sub>5</sub>	2.19	2.10	2.11	2.03
Mo <sub>6</sub> –N <sub>5</sub>	2.19	2.10	2.11	2.03
Mo <sub>9</sub> –N <sub>5</sub>	2.20	2.21	2.23	2.25

**Table 3** continued

Bonds	$\delta$ -MoN	La–MoN(6c)	Gd–MoN(6c)	Yb–MoN(6c)
Mo <sub>17</sub> –N <sub>5</sub>	2.20	2.41	2.35	2.32
Mo <sub>18</sub> –N <sub>5</sub>	2.20	2.21	2.23	2.25
Mo <sub>5</sub> –N <sub>6</sub>	2.15	2.22	2.25	2.15
Mo <sub>8</sub> –N <sub>6</sub>	2.24	2.09	2.11	2.10
Mo <sub>14</sub> –N <sub>6</sub>	2.22	2.37	2.25	2.30
Mo <sub>16</sub> –N <sub>6</sub>	2.17	2.03	2.08	2.08
Mo <sub>17</sub> –N <sub>6</sub>	2.17	2.19	2.18	2.18
Mo <sub>17</sub> –N <sub>7</sub>	2.17	2.19	2.18	2.18
Mo <sub>23</sub> –N <sub>7</sub>	2.22	2.37	2.25	2.30
Mo <sub>24</sub> –N <sub>7</sub>	2.15	2.22	2.25	2.15
Mo <sub>26</sub> –N <sub>7</sub>	2.17	2.03	2.08	2.08
Mo <sub>27</sub> –N <sub>7</sub>	2.24	2.09	2.11	2.10
Mo <sub>14</sub> –N <sub>8</sub>	2.22	2.23	2.25	2.21
Mo <sub>16</sub> –N <sub>8</sub>	2.17	2.12	2.12	2.11
Mo <sub>22</sub> –N <sub>8</sub>	2.15	2.04	2.04	2.03
Mo <sub>23</sub> –N <sub>8</sub>	2.22	2.23	2.25	2.21
Mo <sub>26</sub> –N <sub>8</sub>	2.17	2.12	2.12	2.11

**Table 4** VASP-optimized lattice parameters of  $\delta$ -MoN and Ln–MoN(6c) and the formation energies of Ln–MoN(6c)

Compounds	a ( $\text{\AA}$ )	c ( $\text{\AA}$ )	Volume ( $\text{\AA}^3$ )	$E_f^{\text{Ln}}$ (eV)
$\delta$ -MoN	5.777	5.673	163.99	
La–MoN(6c)	5.920	5.777	175.32	1.5690
Gd–MoN(6c)	5.859	5.754	171.08	-1.3866
Yb–MoN(6c)	5.801	5.697	166.02	-0.4239

The computed formation energies are listed in Table 4. It is found that for the La-doping, the formation energy is 1.569 eV. This large positive value of  $E_f^{\text{La}}$  is a sign that the cohesive energy loss is so large that the doping of the La element is not easy. The formation energies of Gd–MoN and Yb–MoN are all negative, which indicates that the Gd- and Yb-dopings are energetically favorable.

Figure 3 shows the PDOS for the valence states of the Ln, Mo, and N atoms. The profile of the PDOS of  $\delta$ -MoN is in good agreement with that obtained by Zhao et al. [30]. One sees that considerable Mo  $d$ -band hybridizes with the N  $p$ -components for both the undoped and the doped systems. Overall, although  $\delta$ -MoN and Ln–MoN are obviously metals, their bonding might also be said to have a considerable Mo–N covalent component.

For a doped system, the electron redistribution would significantly affect the interatomic bonding. One can obtain directly an insight into the bonding changes induced by the dopings from the charge-density distribution. In Fig. 4, we show the charge-density profiles in the planes containing different atoms for the undoped and the doped systems,

**Fig. 3** Partial densities of states of  $\text{Ln}-4f$ ,  $\text{Mo}-4d$ , and  $\text{N}-2p$  for the undoped  $\delta$ - $\text{MoN}$  and the doped  $\text{Ln}-\text{MoN}(6c)$ . The Fermi level is set as 0.0 eV

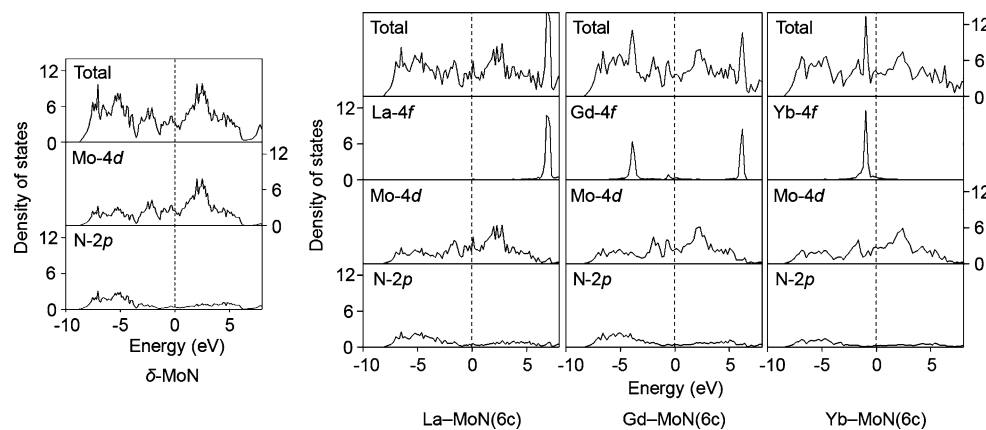
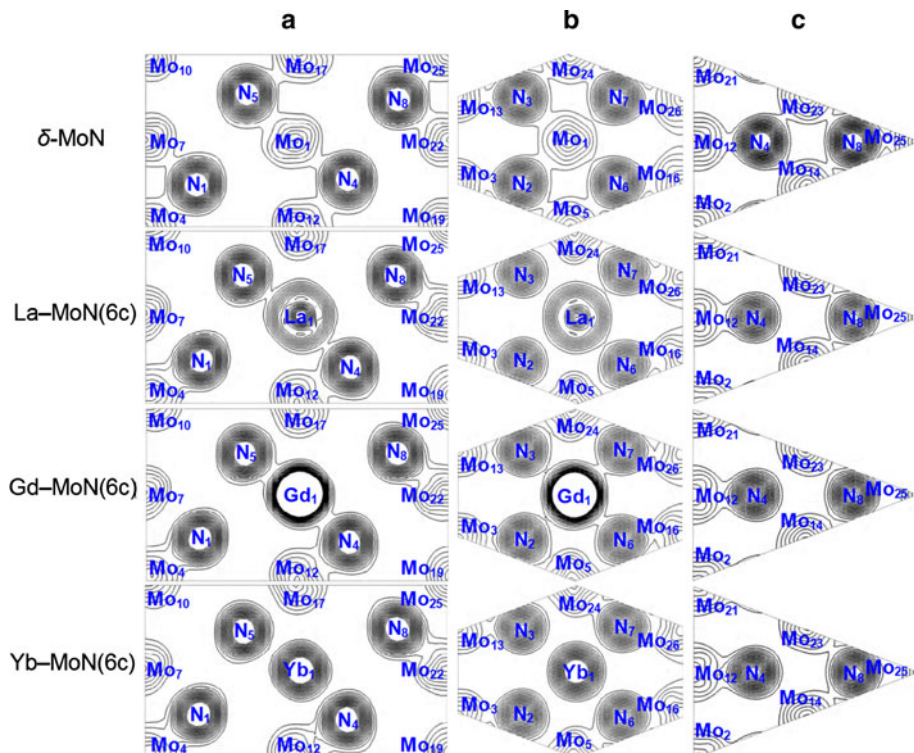


**Fig. 4** The charge-density distributions **a** on the planes containing  $\text{Mo}_1/\text{Ln}_1$  and  $\text{N}_{4,5}$  atoms, **b** on the planes containing  $\text{Mo}_1/\text{Ln}_1$  and  $\text{N}_{2,3,6,7}$  atoms, and **c** on the planes containing  $\text{Mo}_{14,23}$  and  $\text{N}_4$  atoms



from which pronounced differences in the Mo–N and Ln–N bondings can be observed among these four systems. Each N atom forms covalent-like bonds with its neighboring Mo atoms in the undoped  $\delta$ - $\text{MoN}$ , in line with the PDOS result. In the La and Gd-doped systems, evident covalent-like  $\text{Ln}_1-\text{N}_{4,5}$  bonds as well as weak covalent-like  $\text{Ln}_1-\text{N}_{2,3,6,7}$  bonds are found. The doping of La and Gd obviously damage some Mo–N bonds such as the  $\text{Mo}_{14,23}-\text{N}_4$  (c.f. Fig. 4c) and the  $\text{Mo}_{17}-\text{N}_5$  (c.f. Fig. 4a) bonds. This case is expected from the geometry that the bond lengths of  $\text{Mo}_{14,23}-\text{N}_4$  and  $\text{Mo}_{17}-\text{N}_5$  are largely lengthened by the La- and Gd-dopings. For the Yb-doped one, the covalent-like Mo–N bonding is well preserved, but the charge distributions between the Yb and the N atoms are vanishingly small, indicating an ionic component to the Yb–N bonding,

i.e., the Yb atom ionizes  $f$ -electrons toward the N  $p$ -orbitals, which will be further demonstrated in the following section.

### 3.2 Effect on the transport property

In NEGF theory, the current at an applied bias voltage  $V$  through the device is calculated by using Landauer–Büttiker formula [46]:

$$I(V) = G_0 \int_{-\infty}^{+\infty} n(E) T(E, V) dE \quad (3)$$

where  $G_0 = 2e^2/h$  is the quantum unit of conductance,  $h$  is the Plank's constant, and  $T(E, V)$  is the transmission

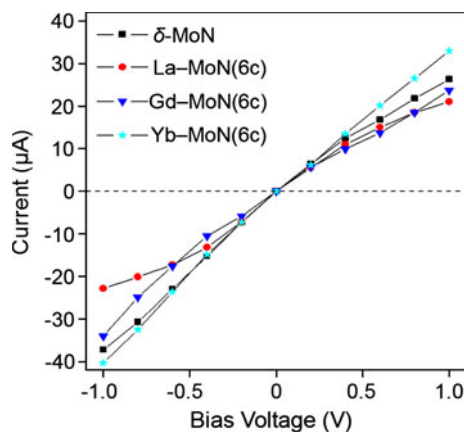


**Fig. 5** The  $I$ - $V$  characteristic of the undoped  $\delta$ -MoN and the doped Ln–MoN(6c) systems self-assembled on the Ag (111) surface

function for electrons with energy  $E$  at certain bias  $V$ . It is described as:

$$T(E, V) = \text{Tr} \left[ \Gamma_L(E, V) G(E, V) \Gamma_R(E, V) G^\dagger(E, V) \right] \quad (4)$$

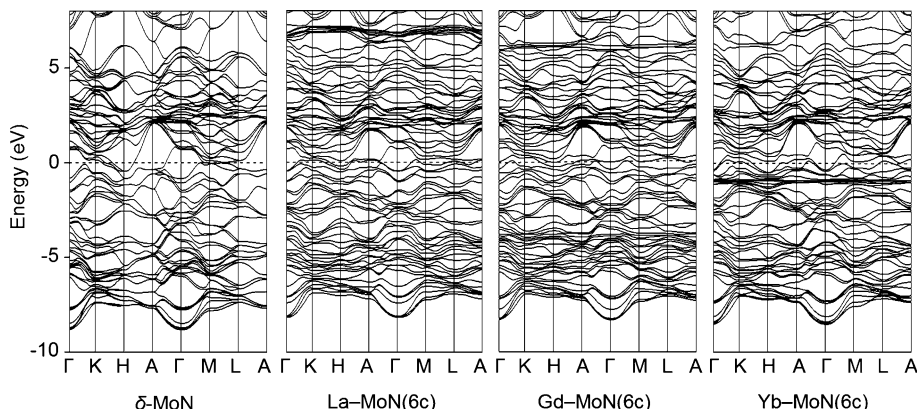
where  $G$  is the Green's function of the scattering region,  $\Gamma_{L/R}$  is the coupling matrix, and  $V$  is the applied bias.  $n(E)$  is written as a function below:

$$n(E) = f(E - \mu_L(V)) - f(E - \mu_R(V)) \quad (5)$$

where  $\mu_L(V)$  and  $\mu_R(V)$  are the electrochemical potentials of the left and right electrodes, respectively.  $\mu_{L/R}(0)$  is the Fermi level, and  $f$  is the Fermi function.

The calculated current–voltage ( $I$ – $V$ ) curves of the undoped and the Ln-doped systems are plotted in Fig. 5. Apparently, different Ln-doping exerts different influence on the conductivity. A clear drop of the conductivity was found after La- and Gd-dopings. On the contrary, the conductivity was improved upon the Yb-doping. Technically, conductivity may be expressed as the product of carrier density and carrier mobility. The former is related to the change of densities of states (DOS) near the Fermi energy level, and the latter to the scattering of the carriers.

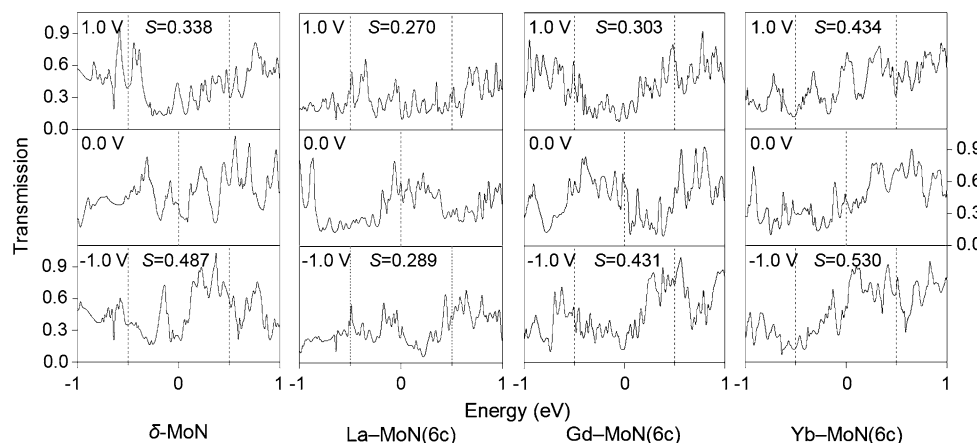
**Fig. 6** VASP-calculated band structures for the undoped  $\delta$ -MoN and the doped Ln–MoN(6c)



The enhancement of the DOS near the Fermi level is beneficial to the increase in carrier density, while the doping of alien atoms into pure  $\delta$ -MoN surely introduces extra carrier scattering which decreases the mobility. It is clear from the  $I$ – $V$  feature that the La-, Gd-, and Yb-dopings affect the transport properties in different manners.

Figure 6 gives the band structures. A metallic nature of these systems is evident, resulting in nearly linear characteristic of the  $I$ – $V$  curves. From Fig. 3, we can see that the Fermi level is mainly dominated by the Mo  $d$ -state in Ln–MoN, which is rather similar to that of the undoped  $\delta$ -MoN. The  $f$ -state of the La, Gd, and Yb atoms contributes localized bands, which inevitably induces a resonant backscattering at the impurity bound state energies. The entirely empty La  $f^0$ -configuration enables its  $f$ -band to embed deeply in the conduction band (ca. 7 eV), indicating that the La-doping cannot effectively increase the carrier density. The decrease in the conductivity of La–MoN can be undoubtedly assigned to the backscattering of incoming wavepackets by the potential well created by the La impurities. Owing to the electron correlation effect, the  $f$ -state of Gd splits into three peaks as shown in Fig. 3: two distinct contributions located around –4 and 6 eV, respectively, and a rather weak contribution near the Fermi level. This splitting was also confirmed by Zhong et al. [47, 48]. Therefore, the charge carrier density cannot be effectively increased by the Gd-doping. The backscattering effect is responsible for the unimproved conductivity of Gd–MoN. As for Yb–MoN, Yb  $f$ -state contributes an evident peak at the top of the valence band due to the full-filled Yb  $f^{14}$ -configuration. The Yb  $f$ -electrons could transfer from the valence band to the Mo  $d$ -conduction band and the N  $p$ -conduction band. Hence, the Yb atom undergoes an ionic-like interaction with its neighboring N atoms, in accordance with the charge-density distributions. The impurity potential could be screened to a certain extent by the  $f$ -carriers, and the extra scattering by the Yb atom may be weak. Therefore, Yb–MoN possesses higher conductivity than  $\delta$ -MoN.

**Fig. 7** Transmission spectrums of the two-probe systems of the undoped  $\delta$ -MoN and the doped Ln–MoN(6c) self-assembled on the Ag (111) surface at bias voltages of 0.0, −1.0, and 1.0 V. The dashed lines indicate the bias window. The integral areas of the resonant peaks within the bias window,  $S$ , are also given



To further investigate the transport properties of these systems, their energy dependences of the transmission spectrums were calculated. As shown in equation (3), the current  $I(V)$  is closely related to the transmission function  $T(E,V)$ . We know that only electrons with some energy near the Fermi level  $[\mu_L(V), \mu_R(V)]$  contribute to the total current. Here,  $[\mu_L(V), \mu_R(V)]$  is usually called bias window. In the ATK program, the Fermi level has been set as 0.0 eV. So the bias window is mainly referred to  $[-V/2, V/2]$  [42]. Therefore, the current can be determined by  $T(E,V)$  in the bias windows indirectly. The larger is the integral area of the resonant peaks within the bias window (denoted as  $S$ ), the higher is the current, and vice versa.

The transmission spectrums at 0.0, −1.0, and 1.0 V applied bias voltages as well as the integral areas of the resonant peaks within the bias window,  $S$ , are shown in Fig. 7. Clearly, the values of  $S$  in La- and Gd-doped systems are reduced compared with the undoped  $\delta$ -MoN in the presence of the same applied bias voltage. A reverse case is found for Yb–MoN. For example, under 1.0 V applied bias, the values of  $S$  are decreased by 0.068 and 0.035 after the La- and Gd-dopings, respectively, while that in Yb–MoN is increased by 0.096. It is noteworthy that the shape of the transmission spectrums changes by different dopings. For example, more sharp resonant peaks within the bias window are found for Gd–MoN. This change, however, is not surprising because the incorporating of a rare earth atom ineluctably alters the effective potential in the scattering region. Figure 8 illustrates the difference of the effective potential between the case where the bias voltage of ±1.0 V is applied and the case of 0.0 V for the undoped  $\delta$ -MoN and the doped Ln–MoN(6c) self-assembled on the Ag (111) surface.

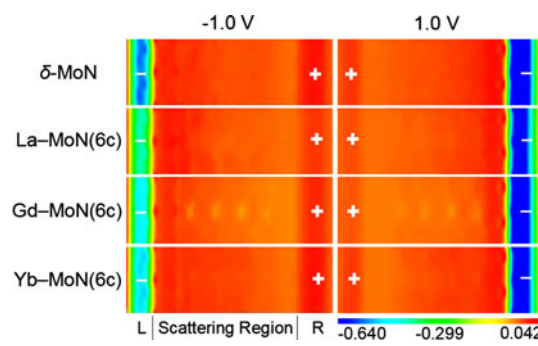


**Fig. 8** Difference of the effective potential between the case where the bias voltage of ±1.0 V is applied and the case of 0.0 V for the undoped  $\delta$ -MoN and the doped Ln–MoN(6c) self-assembled on the Ag (111) surface

#### 4 Conclusions

Combining non-equilibrium Green's function technique with density functional theory, the rare earth element doping effects on the bonding and transport property of  $\delta$ -MoN were theoretically investigated. The Mo–N bond lengths become more uneven after Ln-doping. The  $\text{Mo}_{14,23}\text{N}_4$  and  $\text{Mo}_{17}\text{N}_5$  bonds were heavily lengthened by the La- and Gd-dopings, resulting in an obvious damage of their bonding. The formation energies confirmed that the doping of the La element was not easy while the Gd- and Yb-dopings were energetically favorable. Evident covalent-like La–N and Gd–N bonds were formed in La–MoN and Gd–MoN, respectively, while the Yb atom underwent an ionic-like interaction with its neighboring N atoms in Yb–MoN.

Upon the La- and Gd-dopings, we observed a clear drop of the conductivity. On the contrary, the conductivity was improved upon the Yb-doping. The La- and Gd-dopings could not effectively increase the carrier density near the Fermi level. The decrease in the conductivity of La–MoN and Gd–MoN should be assigned to the backscattering of

incoming wavepackets by the potential well created by the La and Gd impurities. As for Yb–MoN, the Yb *f*-electrons could transfer from the valence band to the Mo *d*-conduction band and the N *p*-conduction band, which is beneficial to improving the conductivity.

**Acknowledgments** The authors thank the NSF of China (51073048), the SF for leaders in academe of Harbin City of China (2010RFJGG016), the SF for Postdoctoral of Heilongjiang province of China (LBHQ07058), and the SF for elitists of Harbin University of Science and Technology for the financial supports.

## References

1. Lévy F, Hones P, Schmid PE, Sanjinés R, Diserens M, Wiemer C (1999) Surf Coat Technol 120–121:284
2. Holleck H (1986) J Vac Sci Technol A 4:2661
3. Suzuki K, Yamaguchi Y, Kaneko T, Yoshida H, Obi Y, Fujimori H, Morita H (2001) J Phys Soc Jpn 70:1084
4. Vandenberg JM, Matthias BT (1974) Mater Res Bull 9:1085
5. Gulbiński W, Suszko T (2006) Surf Coat Technol 201:1469
6. Inumaru K, Baba K, Yamanaka S (2006) Physica B Condensed Matter 383:84
7. Bull CL, Kawashima T, McMillan PF, Machon D, Shebanova O, Daisenberger D, Soignard E, Takayama-Muromachi E, Chapon LC (2006) J Solid State Chem 179:1762
8. Jahn H, Ettmayer P (1978) J Less-Common Met 58:85
9. Matthias BT, Hulm JK (1952) Phys Rev 87:799
10. Inumaru K, Baba K, Yamanaka S (2005) Chem Mater 17:5935
11. Bull CL, McMillan PF, Soignard E, Leinenweber K (2004) J Solid State Chem 177:1488
12. Bezinge A, Yvon K, Muller J (1987) Solid State Commun 63:141
13. Machon D, Daisenberger D, Soignard E, Shen G, Kawashima T, Takayama-Muromachi E, McMillan PF (2006) Phys Status Solidi A 203:831
14. Wang YM, Lin RY (2004) Mater Sci Eng B 112:42
15. Anitha VP, Major S, Chandrashekaram D, Bhatnager M (1996) Surf Coat Technol 79:50
16. Bereznai M, Tóth Z, Caricato AP, Fernández M, Luches A, Majni G, Mengucci P, Nagy PM, Juhász A, Nánai L (2005) Thin Solid Films 473:16
17. Ettmayer P (1970) Montash Chem 101:127
18. Inumaru K, Baba K, Yamanaka S (2006) Phys Rev B 73:052504
19. Chen J, Boyer LL, Krakauer H, Mehl MJ (1988) Phys Rev B 37:3295
20. Yamamoto H, Miki T, Tanaka M (1986) Adv Cryog Eng 32:671
21. Terada N, Nose M, Hoshi Y (1986) Adv Cryog Eng 32:663
22. Saito K, Asada Y (1987) J Phys F Met Phys 17:2273
23. Savvides N (1987) J Appl Phys 62:600
24. Pickett WE, Klein BM, Papaconstantopoulos DA (1981) Physica B 107:667
25. Papaconstantopoulos DA, Pickett WE, Klein BM, Boyer LL (1984) Nature 308:494
26. Papaconstantopoulos DA, Pickett WE, Klein BM, Boyer LL (1985) Phys Rev B 31:752
27. Papaconstantopoulos DA, Pickett WE (1985) Phys Rev B 31:7093
28. Hart GLW, Klein BM (2000) Phys Rev B 61:3151
29. Sahu BR, Kleinman L (2004) Phys Rev B 70:073103
30. Zhao EJ, Wang JP, Wu ZJ (2010) Physica Status Solidi (b) 247:1207
31. Zhao XD, Range KJ (2000) J Alloy Compd 296:72
32. Cendlewska B, Morawski A, Misiuk A (1987) J Phys F Met Phys 17:L71
33. Soignard E, McMillan PF, Chaplin TD, Farag SM, Bull CL, Somayazulu MS, Leinenweber K (2003) Phys Rev B 68:132101
34. Madsen GK, Blaha P, Schwarz K, Sjöstedt E, Nordström L (2001) Phys Rev B 64:195134
35. Perdew JP, Chevary JA, Vosko SH, Jackson KA, Pederson MR, Singh DJ, Fiolhais C (1992) Phys Rev B 46:6671
36. Perdew JP, Wang Y (1992) Phys Rev B 45:13244
37. Kresse G, Joubert D (1999) Phys Rev B 59:1758
38. Blöchl PE (1994) Phys Rev B 50:17953
39. Liechtenstein AI, Anisimov VI, Zaanen J (1995) Phys Rev B 52:R5467
40. Dudarev SL, Botton GA, Savrasov SY, Humphreys CJ, Sutton AP (1998) Phys Rev B 57:1505
41. Taylo J, Guo H, Wang J (2001) Phys Rev B 63:245407
42. Brandbyge M, Mozos JL, Ordejón P, Taylor J, Stokbro K (2002) Phys Rev B 65:165401
43. Soler JM, Artacho E, Gale JD, Garcia A, Junquera J, Ordejón P, Sanchez-Portal D (2002) J Phys Condens Matter 14:2745
44. ATK, Version 2.0, atomistix a/s (2008) [www.atomistix.com](http://www.atomistix.com)
45. Cantele G, Degoli E, Luppi E, Magri R, Ninno D, Iadonisi G, Ossicini S (2005) Phys Rev B 72:113303
46. Landauer R (1957) IBM J Res Dev 1:223
47. Zhong GH, Wang JL, Zeng Z (2008) J Phys Condens Matter 20:295221
48. Losovyj YB, Wooten D, Santana JC (2009) J Phys Condens Matter 21:045602